PAPER

Check for updates

Hydrolytic dehydrogenation of NH₃BH₃ catalyzed by ruthenium nanoparticles supported on magnesium–aluminum layered double-hydroxides

Xueying Qiu, Jiaxi Liu, Pengru Huang, (iD) Shujun Qiu, (iD) Chaoming Weng, Hailiang Chu, (iD) * Yongjin Zou, Cuili Xiang, Fen Xu and Lixian Sun*

Ammonia borane (AB, NH₃BH₃) with extremely high hydrogen content (19.6 wt%) is considered to be one of the most promising chemical hydrides for storing hydrogen. According to the starting materials of AB and H₂O, a hydrogen capacity of 7.8 wt% is achieved for the AB hydrolytic dehydrogenation system with the presence of a highly efficient catalyst. In this work, ruthenium nanoparticles supported on magnesium–aluminum layered double hydroxides (Ru/MgAl-LDHs) were successfully synthesized *via* a simple method, *i.e.*, chemical reduction. The effect of Mg/Al molar ratios in MgAl-LDHs on the catalytic performance for AB hydrolytic dehydrogenation was systematically investigated. Catalyzed by the as-synthesized Ru/Mg₁Al₁-LDHs catalyst, it took about 130 s at room temperature to complete the hydrolysis reaction of AB, which achieved a rate of hydrogen production of about 740 ml s⁻¹ g⁻¹. Furthermore, a relatively high activity (TOF = 137.1 mol$_{H_2}$ mol$_{Ru}$⁻¹ min⁻¹), low activation energy (E_a = 30.8 kJ mol⁻¹) and fairly good recyclability of the Ru/Mg₁Al₁-LDHs catalyst in ten cycles were achieved toward AB hydrolysis for hydrogen generation. More importantly, the mechanism of AB hydrolysis catalyzed by Ru/MgAl-LDHs was simulated *via* density functional theory. The facile preparation and high catalytic performance of Ru/MgAl-LDHs make it an efficient catalyst for hydrolytic dehydrogenation of AB.

1. Introduction

Hydrogen is considered a very clean energy carrier due to its high efficiency and power density, and its limited environmental impact.[1] One of the key issues for hydrogen as a promising energy carrier is to develop suitable solid-state hydrogen storage materials with the desirable properties of high hydrogen capacity and controllable release rate, acceptable air stability, relative nonflammability, and low toxicity.[2–4] Among many chemical hydrides, ammonia borane (AB, NH₃BH₃) has recently attracted considerable attention as a potential hydrogen storage material due to its extremely high hydrogen content (19.6 wt%), low molecular weight (30.86 g mol⁻¹), and environmentally friendly nature.[5–12] Hydrogen can be released from AB by thermolysis or solvolysis in the presence of suitable catalysts.[13] However, the former process has some drawbacks: (i) it requires a very long induction time and high temperature for complete hydrogen release, and (ii) various by-products, such as ammonia (NH₃) and borazine (B₃N₃H₆), can be formed during reaction for releasing hydrogen.[14] Relatively

speaking, hydrolyzation is an effective way to produce hydrogen from AB at room temperature because of the simple operation and low pollution.

As is known to all, AB is very stable at room temperature and can react with water to quickly release hydrogen with an assistance of metal catalysts. Many metals show high catalytic activity toward the hydrolysis of AB, among which precious metals are mainly Ru,[15,16] Pt,[17] Pd,[18] and Rh[19] and non-precious metals are mainly Co and Ni.[20,21] Unfortunately, these monometallic catalysts with very small size in nano-size scale often face severe agglomeration, resulting in poor stability and activity.[22] Hence the supports are always employed to disperse and stabilize these metal particles, especially for metal particles with size in nanometers. Therefore, through the interaction of metal particles and supports, the performance of supported metal catalysts will be significantly improved. Commonly used carriers are carbon black,[23] CNTs,[24] graphene,[25] SiO₂,[26] Al₂O₃,[27] and MOFs.[28] However, as the catalytic reaction proceeds, the supported metal nanoparticles on these preceding carriers will also inevitably agglomerate, which results in the deterioration of the reaction activity.[29] Thus the supports that has moderate interaction with metal particles have been developed.

Layered double hydroxides (LDHs) are a class of anionic clay minerals following the general chemical formula of $[M_{1-x}^{2+}M_x^{3+}(OH)_2]^x[A^{n-}]_{x/n}\cdot yH_2O$,[30] which have an anion-exchange capability featured with lamellar structure.[31] LDHs

Guangxi Key Laboratory of Information Materials, Guangxi Collaborative Innovation Center of Structure and Property for New Energy and Materials, School of Materials Science and Engineering, Guilin University of Electronic Technology, Guilin, 541004, P. R. China. E-mail: chuhailiang@guet.edu.cn; sunlx@guet.edu.cn; Fax: +86-773-2290129; Tel: +86-773-2216607

have high zero charge, rich layered surface of OH^-, and adjustable surface alkali acid. This is the main reason why we choose LDHs as the carrier in this study. For example, the zero charge point of the MgAl-LDHs carrier is between pH = 7 and 8, and the surface of the carrier is positively charged when the pH of the suspension is between 5 and 7. Thus, the carrier has a strong ability to adsorb the metal particles. When the pH of the suspension is more than 8, the adsorption capacity of the carrier to the metal particles becomes very weak.[32] So, Mg^{2+} and Al^{3+} have the ability to regulate the surface charge of LDHs. Therefore, with brucite layer cationic modulation, high adsorption and other advantages, they are widely used as adsorbent, electrochemical material accelerator and catalyst.[33,34] In addition, as a carrier of catalysts, a large number of hydroxyl groups exist on the surface of MgAl-LDHs to anchor metal particles, which reduces the phenomenon of particle agglomeration and increases the adsorption of metal particles.

In this work, we used magnesium–aluminum layered double hydroxides (MgAl-LDHs) as the carrier to support ruthenium nanoparticles for hydrolytic dehydrogenation of AB. The results showed that Ru nanoparticles supported by MgAl-LDHs had higher catalytic activity, superior cyclic stability and lower activation energy toward AB hydrolysis.

2. Experimental section

2.1 Materials

AB (NH_3BH_3, 90 wt%) and ruthenium(III) chloride hydrate ($RuCl_3 \cdot nH_2O$, 35–42 wt% Ru basis) were purchased from Aladdin Inc. (Shanghai, China). Magnesium nitrate ($Mg(NO_3)_2 \cdot 6H_2O$), aluminum nitrate ($Al(NO_3)_3 \cdot 9H_2O$), and urea were obtained from Xilong Scientific Co., Ltd. All chemicals are analytically pure and were used without further refinement. The deionized water used in this study was produced from the reverse osmosis and the following ion-exchange and filtration.

2.2 Preparation of MgAl-LDHs and Ru/MgAl-LDHs

Hydrothermal method was employed to synthesize MgAl-LDHs with different Mg/Al molar ratios by changing the relative amount of $Al(NO_3)_3 \cdot 9H_2O$ and $Mg(NO_3)_2 \cdot 6H_2O$. Typically for the synthesis of Mg_1Al_1-LDHs, 2 mmol of $Mg(NO_3)_2 \cdot 6H_2O$, 2 mmol of $Al(NO_3)_3 \cdot 9H_2O$, and 30 mmol of urea were added into 50 ml of deionized water for ultrasonic dispersion for 10 min. The resulting solution was put into a 70 ml Teflon-lined autoclave, which was then sealed and placed in an oven upon heating treatment at 120 °C for 24 h. After the reaction was completed, the product was obtained by centrifugation with deionized water for several times, and then dried overnight in an oven at 80 °C. Urea here has the ability to regulate alkalinity, and it is also used as a precipitator. When $Mg_{0.5}Al_1$-LDHs, Mg_2Al_1-LDHs, and Mg_3Al_1-LDHs were synthesized, only the amount of $Mg(NO_3)_2 \cdot 6H_2O$ was changed from 2 mmol to 1, 4 and 6 mmol, respectively, under the same conditions.

Ru/MgAl-LDHs was synthesized by a chemical reduction method. In simple terms, 0.02 mmol of $RuCl_3 \cdot nH_2O$ and 100 mg of each MgAl-LDHs sample were added to 20 ml of deionized water. For the mixture solution, ultrasonic dispersion was performed for 15 min and moderate stirring for 12 h. Then 20 ml of AB homogenous aqueous solution (70 mg, 2.2 mmol) was quickly injected into the well-mixed solution mentioned above for reducing Ru^{3+} into Ru nanoparticles. Finally, Ru/MgAl-LDHs catalysts were obtained by filtration. In order to investigate the effect of Ru amount on catalytic performance, the amount of $RuCl_3 \cdot nH_2O$ was changed from 0.02 mmol to 0.005 mmol.

2.3 Sample characterization

A Bruker D8 Advance X-ray diffractometer with Cu Kα source (40 kV, 40 mA) was employed to determine the phase structure of the as-prepared samples. The chemical constituents of samples were determined on was performed on a X-ray photoelectron spectrometry (XPS, ESCALAB250Xi, VG Escalab 220i-XL) coupled with Al Kα source. Transmission electron microscope (TEM, Talos F200X) and scanning electron microscope (SEM, QUANTA 450 FEG) were used to characterize the sample morphologies. In addition, the elemental composition of the catalysts was evaluated using energy dispersive X-ray spectroscopy (EDX) that was equipped on TEM. Determination of accurate Ru content was conducted on an inductively coupled plasma mass spectrometry (ICP, Agilent ICP-OES730).

2.4 Catalytic hydrolysis of AB and recycling stability test

Generally, the hydrolysis reaction was carried out at 298 K. By using a syringe, AB aqueous solution (70 mg, 2.2 mmol) was added into a three-necked, round-bottomed flask containing
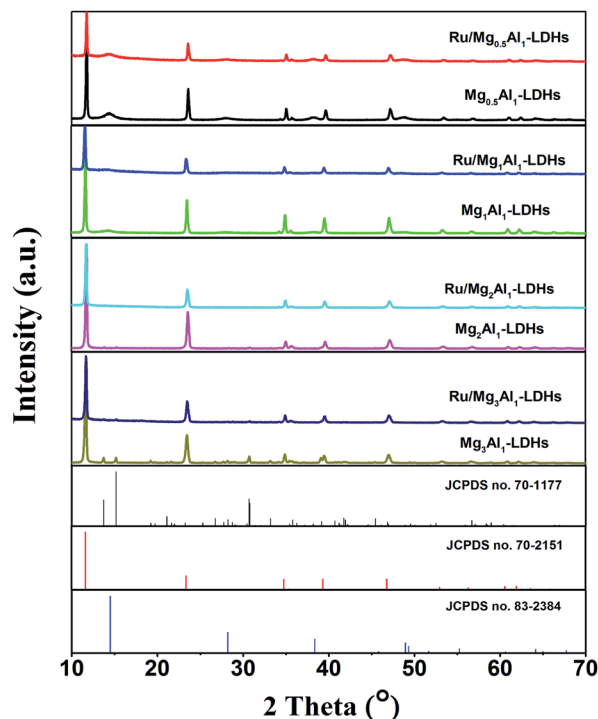

Fig. 1 XRD patterns of pristine MgAl-LDHs samples and Ru/MgAl-LDHs catalysts.

Ru/MgAl-LDHs catalyst, and the catalytic reaction of hydrogen production was performed under vigorous stirring. The volume of produced hydrogen was determined based on the mass of the displaced water. In order to study the reaction kinetics, the hydrolysis of AB catalyzed by Ru/Mg$_1$Al$_1$-LDHs was carried out at the different temperatures (293, 303, 313 and 323 K).

For the recyclability test of the selected high-performance catalyst, Ru/Mg$_1$Al$_1$-LDHs was recycled from the reacted suspension by filtration, washing for many times and then drying under vacuum at 80 °C after each run of hydrogen production reaction was finished. Another new batch of AB aqueous solution (70 mg, 2.2 mmol) was injected into the flask that contained the recyclable Ru/Mg$_1$Al$_1$-LDHs catalyst. The same operation was repeated 10 times at room temperature for testing the recycling stability of the catalyst.

2.5 Theoretical calculations

To deeply understand the promotion effects of the Ru/Mg$_1$Al$_1$-LDHs toward the AB hydrolysis, the theoretical simulation based on DFT method was carried out. All the calculations were based on the density functional theory (DFT) using the projector augmented wave (PAW) pseudopotential as implemented in the Vienna *Ab initio* Simulation Package (VASP).[35–37] For the exchange–correlation potential, we applied Perdew Burke Ernzerhof (PBE) functional within the generalized gradient approximation (GGA).[38,39] The plane-wave cutoff energy for the wave-functions was set to 450 eV, and the Brillouin zone is sampled by a set of $5 \times 5 \times 1$ k-points for the static total energy calculations. The dipole moment correction in the z-direction was considered to eliminate the total dipole moment of the cell. The dispersion-corrected density functional theory (DFT-D2) method in the Grimme scheme has been used in all the calculations.[40] A Ru (001) and Ru cluster on MgAl-LDH were built, and then H$_2$O and O + OH groups were adsorbed on the Ru (001) and Ru/MgAl-LDH, respectively. A vacuum region of 15 Å was used to avoid interface interaction. The convergence of energy and force is within 1×10^{-5} eV and 0.02 eV Å^{-1}, respectively.

3. Results and discussion

3.1 Characterization of Ru/MgAl-LDHs catalyst

In order to explore the crystal structure of the samples, we carried out XRD analysis of MgAl-LDHs before and after loading Ru. As shown in Fig. 1, XRD patterns of pristine MgAl-LDHs show narrow, symmetrical and strong characteristic diffraction peaks at $2\theta = 11.6°$, $23.5°$, $34.9°$, $39.5°$ and $47.0°$. This is
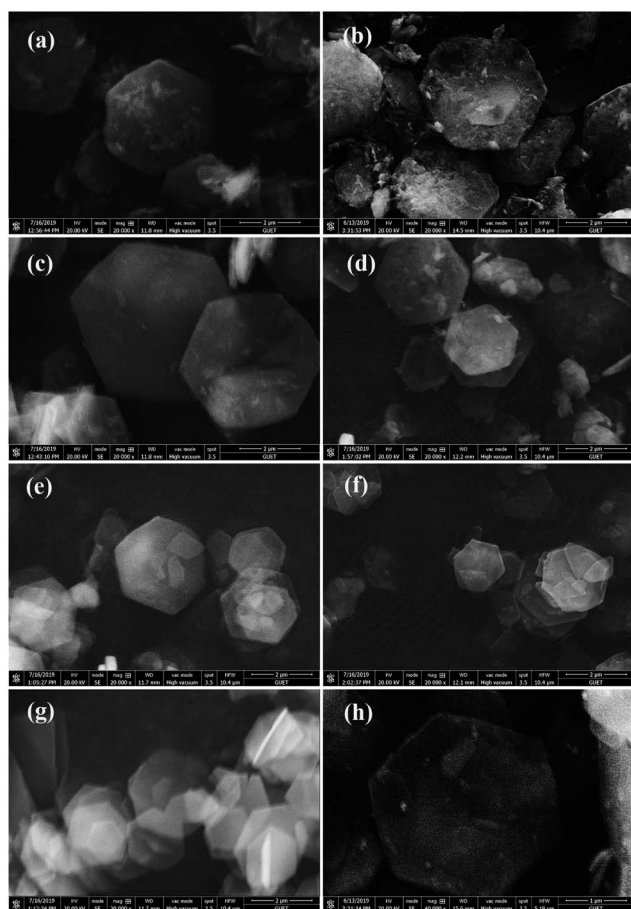

Fig. 2 SEM images: (a) Mg$_{0.5}$Al$_1$-LDHs, (b) Ru/Mg$_{0.5}$Al$_1$-LDHs, (c) Mg$_1$Al$_1$-LDHs, (d) Ru/Mg$_1$Al$_1$-LDHs, (e) Mg$_2$Al$_1$-LDHs, (f) Ru/Mg$_2$Al$_1$-LDHs, (g) Mg$_3$Al$_1$-LDHs, (h) Ru/Mg$_3$Al$_1$-LDHs.
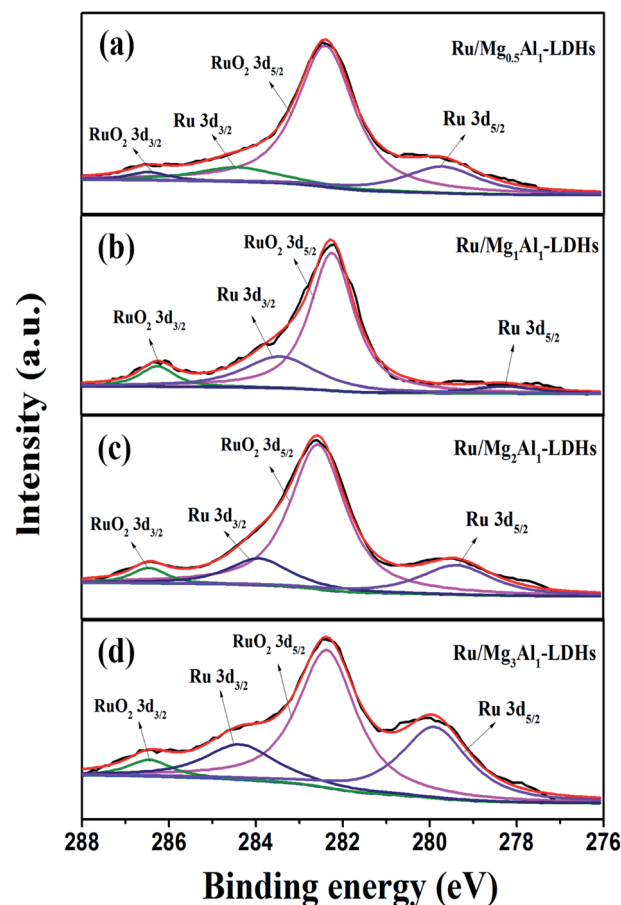
Fig. 3 High-resolution XPS spectra of Ru 3d: (a) Ru/Mg$_{0.5}$Al$_1$-LDHs, (b) Ru/Mg$_1$Al$_1$-LDHs, (c) Ru/Mg$_2$Al$_1$-LDHs, (d) Ru/Mg$_3$Al$_1$-LDHs.
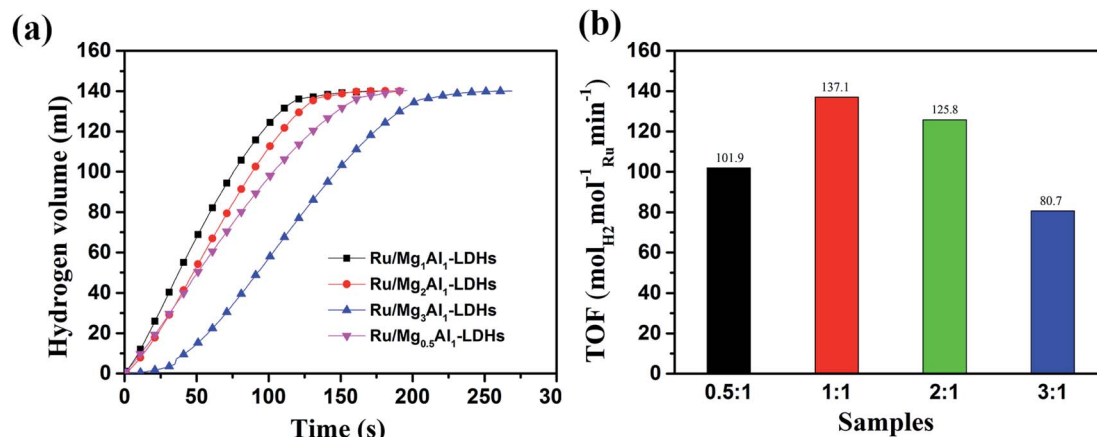
Fig. 4 (a) Hydrolysis performance of AB catalyzed by Ru/MgAl-LDHs at 298 K. (b) Corresponding TOF histograms of Ru/MgAl-LDHs with different proportions.

well consistent with the crystal structure of hydrotalcite (JCPDS no. 70-2151),[41] which indicates the successful synthesis of MgAl-LDHs. Close observation reveals that boehmite (AlO(OH), JCPDS no. 83-2384) is formed in $Mg_{0.5}Al_1$-LDHs sample due to the excess amount of $Al(NO_3)_3 \cdot 9H_2O$. With the increasing amount of $Mg(NO_3)_2 \cdot 6H_2O$, hydromagnesite ($Mg_5(CO_3)_4(OH)_2 \cdot 4H_2O$, JCPDS no. 70-1177) is found in Mg_2Al_1-LDHs and Mg_3Al_1-LDHs samples. As catalyst support of Ru for AB hydrolysis, these impurity phases in MgAl-LDHs would affect the catalytic activity, which will be discussed in the following parts. After supporting Ru particles on MgAl-LDHs through *in situ* reduction, the diffraction peaks of Ru/MgAl-LDHs catalysts exhibited no obvious difference except for the peak intensity. In addition, no crystallization peaks of metallic Ru are found, which may be due to its much lower content (4.6 wt% Ru in Ru/Mg_1Al_1-LDHs determined by ICP). Moreover, the small particle size and the uniform dispersion of ruthenium particles are also responsible for the undetectable diffraction peaks.

The surface morphology of MgAl-LDHs and Ru/MgAl-LDHs samples was studied by SEM. As shown in Fig. 2, pristine MgAl-LDHs samples exhibit hexagonal structures with smooth surfaces. It is worthy to note that Ru/MgAl-LDHs catalysts also show regular hexagonal structure, indicating that there is no variation of the morphology before and after loading Ru particles. However, compared with MgAl-LDHs, the surface of Ru/MgAl-LDHs catalysts become rough after supporting Ru particles, in which there is the most pronounced surface roughness for Ru/$Mg_{0.5}Al_1$-LDHs probably due to the dissolution of boehmite during the loading of Ru particles by chemical reduction.

The chemical constituents of Ru/MgAl-LDHs catalysts were characterized by X-ray photoelectron spectroscopy (XPS). As shown in Fig. 3, curve fittings of Ru 3d core level show that Ru(0) and RuO_2 rather that Ru(III) are observed for all four catalysts. The characteristic peaks of Ru $3d_{3/2}$ and $3d_{5/2}$ are at about 284 eV and 280 eV, indicating that $RuCl_3$ is successfully reduced

Table 1   Catalytic activity of various catalysts for AB hydrolysis reported

Catalysts	Content of AB (mmol)	TOF ($mol_{H_2} \, mol_M^{-1} \, min^{-1}$)	E_a (kJ mol^{-1})	References
Ru/γ-Al_2O_3	1	77	23	17
Ru/graphene	1	100	11.7	25
Ru/carbon black	6	429.5	34.8	23
Ru(0)/MIL-96	1	231	47.7	43
Ru(0)/CeO_2	1	361	51	44
Ru@SiO_2	6	200	38.2	26
Ru/NPC	1	813	24.94	51
Pt/γ-Al_2O_3	1	308	21	17
Pt/CeO_2	1	182	—	45
Pd/$CoFe_2O_4$	1	290	42	46
Ni@h-BN	1	4.1	47.3	47
Ni/C	2	8.8	28	48
Co/Al_2O_3	1	2	62	49
Co/graphene	1	13.9	32.72	50
Ru/Mg_1Al_2-LDHs	2.2	101.9	—	This work
Ru/Mg_1Al_1-LDHs	2.2	137.1	30.8	This work
Ru/Mg_2Al_1-LDHs	2.2	125.8	—	This work
Ru/Mg_3Al_1-LDHs	2.2	80.7	—	This work

to Ru(0) through chemical reduction by AB. Unfortunately, here the C 1s peak overlaps with the Ru $3d_{3/2}$ peak. However, the characteristic peaks of RuO_2 $3d_{3/2}$ and $3d_{5/2}$ appears near 286.2 eV and 282 eV, which was mainly attributed to oxidation of some Ru particles during sample preparation.

Fig. 4(a) shows the hydrolysis performance of AB catalyzed by Ru/MgAl-LDHs catalysts at 298 K. It shows that the volume of released hydrogen catalyzed by Ru/MgAl-LDHs with different Mg/Al molar ratios could reach 88% of the theoretical value. Obviously, Ru/Mg_1Al_1-LDHs could catalyze AB for very rapid hydrogen production in 130 s at room temperature to achieve a high hydrogen release rate of 740 ml s^{-1} g^{-1}, showing superior catalytic activity. For the case of Ru/$Mg_{0.5}Al_1$-LDHs, Ru/Mg_2Al_1-LDHs and Ru/Mg_3Al_1-LDHs, it needs about 180 s, 140 s and 230 s at room temperature to complete hydrogen release, respectively. Therefore, the hydrogen release rates are in the order of Ru/Mg_1Al_1-LDHs > Ru/Mg_2Al_1-LDHs > Ru/$Mg_{0.5}Al_1$-LDHs > Ru/Mg_3Al_1-LDHs. This can be related to two possible factors. One is the high purity of Mg_1Al_1-LDHs without the

formation of boehmite (AlO(OH)) or hydromagnesite ($Mg_5(CO_3)_4(OH)_2 \cdot 4H_2O$), which is confirmed by the aforementioned XRD results. The other one can be ascribed to more Brønsted acid sites in Mg_1Al_1-LDHs,[55] which could reduce the interaction between the support and Ru nanoparticles to exhibit more active sites from metallic state of Ru. This is another essential factor to the rapid rate of AB hydrolysis. Fig. 4(b) shows the corresponding TOF histograms of Ru/MgAl-LDHs catalysts. TOF of Ru/Mg_1Al_1-LDHs is determined to be 137.1 mol_{H_2} mol_{Ru}^{-1} min^{-1}, which is much higher than that of other three catalysts and also higher than many TOF values reported in the literature in Table 1. The reason may be due to the influence of Ru oxidation degree on its catalytic activity. Ru nanoparticles have different crystalline phases. Ru/MgAl-LDHs catalysts of fcc and hcp have different catalytic activities. Compared with the Ru nanoparticles of hcp, the fcc Ru nanoparticles are more easily oxidized and have strong binding ability with OH.[42]

In order to further study the microstructure and element distribution of the samples, Ru/Mg_1Al_1-LDHs with the best
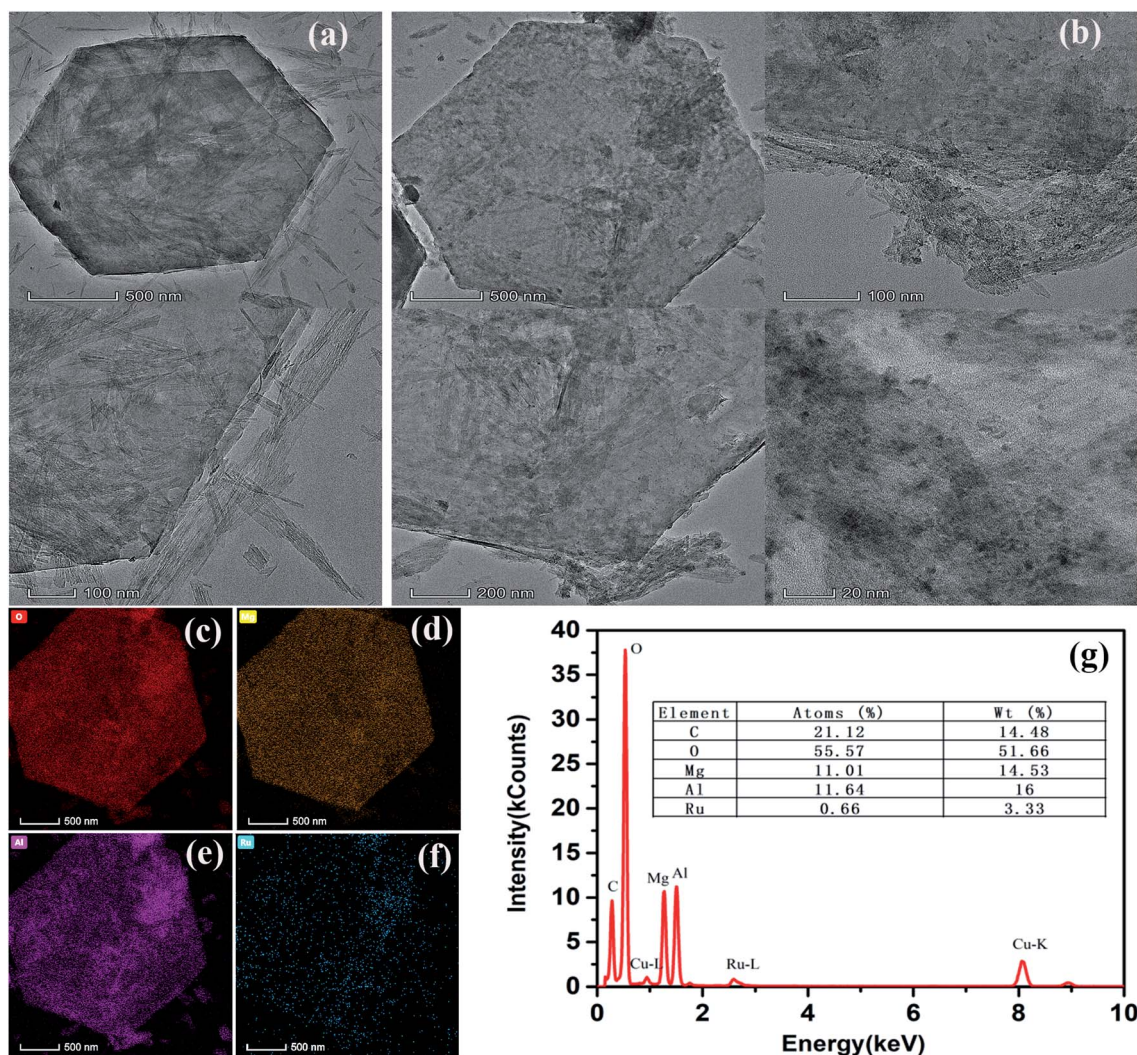

Fig. 5 TEM images: (a) Mg_1Al_1-LDHs and (b) Ru/Mg_1Al_1-LDHs catalyst. STEM-elemental mapping of O (c), Mg (d), Al (e), Ru (f) distribution within the Ru/Mg_1Al_1-LDHs catalyst. (g) EDX spectrum of Ru/Mg_1Al_1-LDHs catalyst.

catalytic performance was selected as the representative sample for TEM characterizations (Fig. 5). As a contrast shown in Fig. 5(a and b), pristine Mg_1Al_1-LDHs shows a regular hexagon lamellar structure with smooth surface. After chemical reduction of $RuCl_3$, we can clearly see from Fig. 5(c–f) that there are many evenly dispersed Ru nanoparticles on the surface of Ru/Mg_1Al_1-LDHs catalyst. The morphology of Mg_1Al_1-LDHs supported on Ru nanoparticles remained unchanged, which is consistent with SEM results. The results showed that, using Mg_1Al_1-LDHs as the carrier, ruthenium nanoparticles on its surface were uniformly dispersed with the particle size of about 3 nm. STEM-mapping clearly showed that the elements of O, Mg, and Al existed in LDHs tablets. Fig. 5(f) showed that Ru nanoparticles were uniformly dispersed on the surface of LDHs. The corresponding EDX spectrum also confirms the existence of C, O, Mg, Al and Ru elements (Fig. 5(g)). The molar ratio of Mg to Al is 14.53 : 16, very close to stoichiometric ratio of 1 : 1, which proves that the chemical composition of Mg_1Al_1-LDHs is unchanged during chemical reduction. The content of Ru nanoparticles measured by EDX spectroscopy was 3.33 wt%, which is slightly lower than that from ICP.

Cyclic stability of Ru/Mg_1Al_1-LDHs catalyst for AB hydrolysis is shown in Fig. 6(a). The results showed that it needed only 250 s to complete the hydrolysis reaction at the 10th cycle, indicating Ru/Mg_1Al_1-LDHs catalyst had superior cyclic stability. Although this, the catalytic activity of Ru/Mg_1Al_1-LDHs catalyst was deteriorated as the cyclic test progresses. As shown in Fig. 6(b), there is still about 58.1% of catalytic activity after 10 times for Ru/Mg_1Al_1-LDHs catalyst, compared to the initial test. TEM images of Ru/Mg_1Al_1-LDHs catalyst after 10 cycles (Fig. 6(c–e)) showed an obvious agglomeration of ruthenium nanoparticles, which could worsen the catalytic effect. This can be attributed to the increased solubility of metaborate as a by-product of AB during the hydrolysis process. Metaborate can be adsorbed on the surface of Ru nanoparticles, limiting their active sites, and increasing the concentration of the solution after repeated hydrolysis. It may hinder the diffusion of AB and the collision between AB and Ru nanoparticles, thereby reducing the catalytic activity.[51] In addition, the gradual attenuation of catalytic activity can also be attributed to the partial loss of ruthenium nanoparticles resulting from multiple filtration and washing for catalyst recycling.

Ru/Mg_1Al_1-LDHs catalysts with different Ru loadings were synthesized by changing the addition amount of $RuCl_3 \cdot nH_2O$ (0.005 mmol, 0.010 mmol, 0.015 mmol, and 0.02 mmol) with the same content of Mg_1Al_1-LDHs carrier (100 mg). As shown in Fig. 7(a), with the increase of the loading mass of Ru nanoparticles, the reaction time of AB hydrolysis was decreased and the hydrogen release rate was increased. Based on Fig. 7(a), the kinetic curve of ln k vs. $\ln[C_{Ru}]$ for catalytic hydrolysis was fitted (Fig. 7(b)). The slope of this curve was determined to be 1.87, indicating a first-order reaction kinetics with respect to the catalyst concentration.
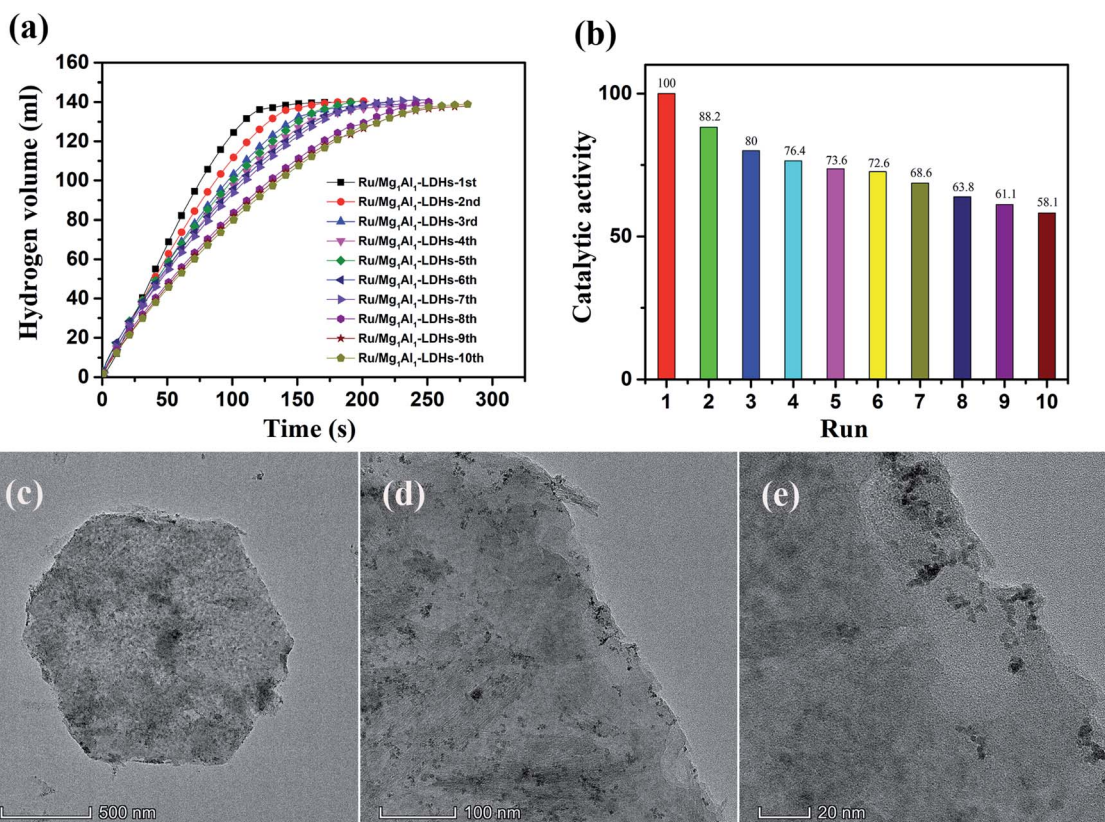

Fig. 6 (a) Cyclic test and (b) catalytic activity of Ru/Mg_1Al_1-LDHs for AB hydrolysis for 10 cycles. (c–e) TEM images of Ru/Mg_1Al_1-LDHs catalyst after 10 cycles.
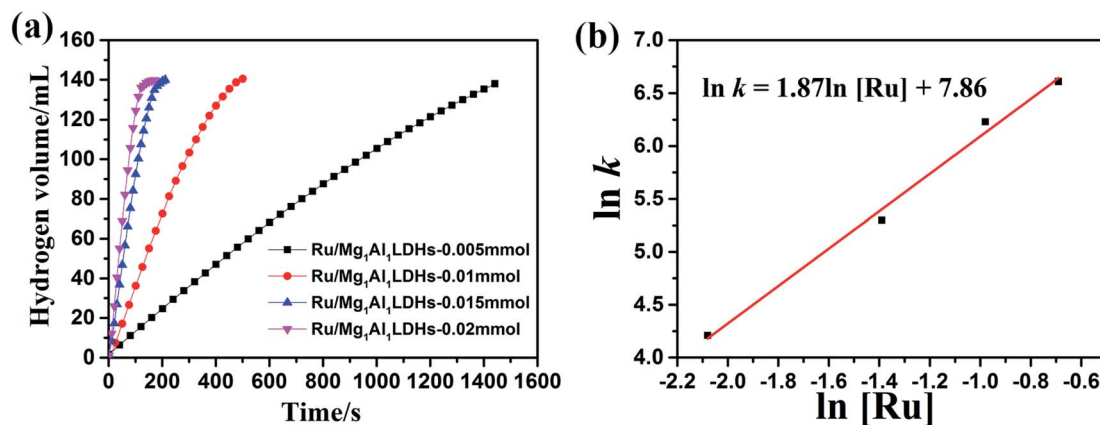
Fig. 7 (a) Influence of Ru/Mg$_1$Al$_1$-LDHs catalyst concentration on catalytic performance at room temperature. (b) Corresponding ln k vs. ln[C$_{Ru}$].

Fig. 8(a) illustrates the volume of generated hydrogen *versus* reaction time for the hydrolytic dehydrogenation of AB catalyzed by Ru/Mg$_1$Al$_1$-LDHs catalyst at different temperatures. This means that the higher reaction temperature, the higher catalytic activity. At high temperature of 323 K, the hydrolysis reaction is completed in only about 40 s. The Arrhenius plot of ln k *versus* 1/T for Ru/Mg$_1$Al$_1$-LDHs catalyst is plotted in Fig. 8(b). From the slop of the straight line, the activation energy (E_a) for the hydrolytic dehydrogenation of AB is calculated to be about 30.8 kJ mol^{-1}, which is lower than most of the reported E_a values of many different catalysts (Table 1).

To further clarify the above conclusions, DFT calculation was performed to deeply understand the promotion effects of the Ru/MgAl-LDH interface toward the AB hydrolysis. Firstly, the structural optimization revealed that Ru cluster could be anchored on the surface of MgAl-LDH to maintain the stable structure with adsorption energy of −23.47 eV. In general, the high-activity catalysts toward AB hydrolysis should have a proper adsorption energy for the adsorption of AB molecules and H$_2$O molecules, and a low dissociation energy of H$_2$O molecule is also indispensable.[52] The adsorption energy of AB

molecule on the surface of Ru (001) surface and the Ru/MgAl-LDH catalyst was optimized (Fig. 9(a and b)). Unfortunately, the optimized geometry structure of AB adsorption on Ru (001) surface have largely deformed and thus the adsorption energy is positive (+1.52 eV). Note that the optimized geometry structure of AB adsorption on the Ru/MgAl-LDH catalyst is relatively stable and adsorption energy is determined to be −1.26 eV. Furthermore, the adsorption of H$_2$O molecule on the Ru (001) surface and the Ru/MgAl-LDH catalyst was also calculated (Fig. 9(c)). Our calculations showed that, compared with the adsorption energy of H$_2$O molecule on the Ru (001) surface (−0.77 eV), a much higher value of −1.59 eV is achieved for the Ru/MgAl-LDH catalyst, indicating the Ru/MgAl-LDH catalyst is more ready for the adsorption of H$_2$O molecules. This may be attributed to the more unpaired electrons of Ru on the Ru/MgAl-LDH catalyst, which will be conducive to the adsorption of H$_2$O and AB molecules. Taking into consideration of the activation of water molecules as rate-determined step for AB hydrolysis,[53,54] we have simulated the reaction pathway of the activation for the water molecule in the reaction of AB hydrolysis, which is shown in Fig. 9(c). The results showed that, compared to the stable
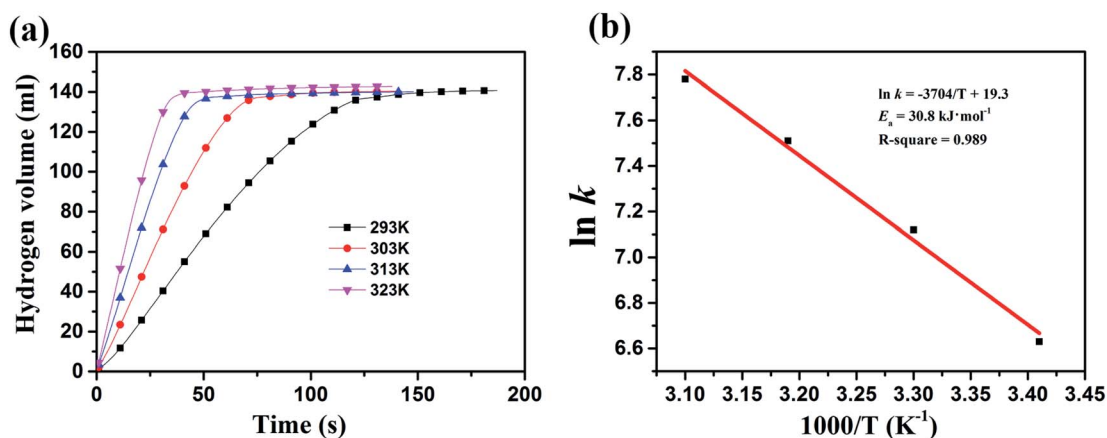

Fig. 8 (a) Hydrogen production of AB solution catalyzed by Ru/Mg$_1$Al$_1$-LDHs catalyst at different temperatures and (b) Arrhenius plot of ln k versus 1/T.
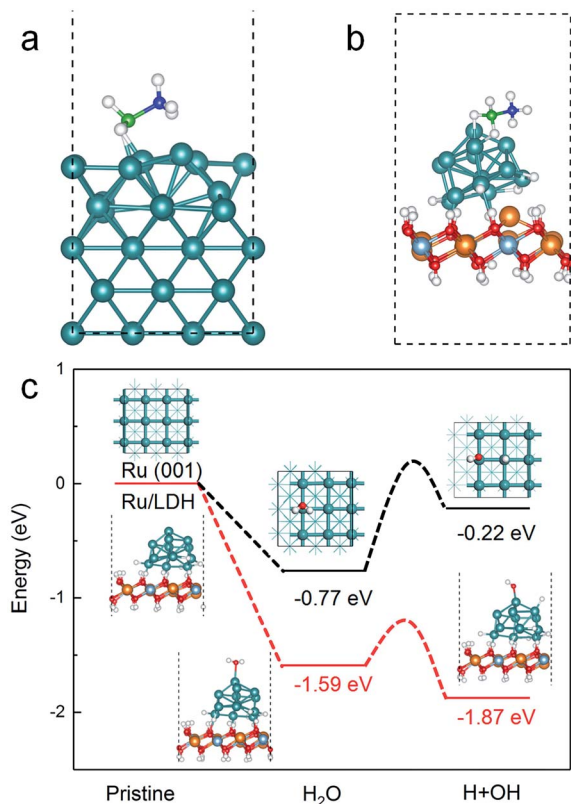
Fig. 9 Optimized geometries for the adsorption of AB molecule on (a) Ru (001) surface and (b) Ru/LDH interface from the side view. (c) Calculated adsorption energy potential profiles of H_2O cleavage on the Ru surface (black line) from the top view and the Ru/LDH surface (red line) from the side view. The dark-green, orange, blue, red, and white balls represent Ru, Mg, Al, O, and H atoms, respectively.

geometry of H_2O, the final energy for H_2O cleavage was decreased to be -1.87 eV at Ru/MgAl-LDH while it was increased to be -0.22 eV at Ru (001), indicating that the Ru/LDH catalyst has the beneficial electronic properties to accelerate the H_2O cleavage rate to form O–H bond. Hence it can be concluded that the Ru/LDH catalyst could facilitate the adsorption of AB and water and then promote the activation of water molecule during AB hydrolysis process. Thus the hydrogen could be easily produced from the reaction of AB and water in our work.

4. Conclusions

In summary, we have successfully prepared a catalyst of Ru nanoparticles supported on MgAl-LDHs by *in situ* reduction method. Used for the hydrolytic dehydrogenation of AB, Ru/Mg_1Al_1-LDHs exhibited superior catalytic performance with high activity (TOF = 137.1 mol_{H_2} $mol_{Ru}^{-1}\cdot min^{-1}$) and low activation energy (E_a = 30.8 kJ mol^{-1}). In addition, it also showed a satisfactory recyclability and retained 58.1% of the initial catalytic activity after 10 times of hydrolysis test. This can be ascribed to the fact that MgAl-LDHs as carrier could provide more active sites of metal Ru nanoparticles and suppress the

agglomeration of Ru nanoparticles. Theoretical calculation confirmed that the Ru/LDH catalyst could facilitate the adsorption of AB and water and then promote the activation of water molecule during AB hydrolysis process. The simple preparation and the high catalytic performance renders Ru/Mg_1Al_1-LDHs a potentially efficient catalyst for the hydrolytic dehydrogenation of AB.

Conflicts of interest

There are no conflicts of interest to declare.

Acknowledgements

References

1 L. Schlapbach and A. Züttel, Hydrogen-storage materials for mobile applications, *Nature*, 2001, **414**, 353–358.

2 S. Qiu, X. Ma, E. Wang, H. Chu, Y. Zou, C. Xiang, F. Xu and L. Sun, Improved dehydrogenation properties of 2LiNH2-MgH2 by doping with Li3AlH6, *Metals*, 2017, **7**(2), 34.

3 S. Qiu, H. Chu, Y. Zou, C. Xiang, F. Xu and L. Sun, Light metal borohydrides/amides combined hydrogen storage systems: composition, structure and properties, *J. Mater. Chem. A*, 2017, **5**(48), 25112–25130.

4 S. Qiu, X. Ma, E. Wang, H. Chu, J. Huot, Y. Zou, C. Xiang, F. Xu and L. Sun, Enhanced hydrogen storage properties of 2LiNH2/MgH2 through the addition of Mg(BH4)2, *J. Alloys Compd.*, 2017, **704**, 44–50.

5 Z. H. Lu, Q. Yao, Z. Zhang, Y. Yang and X. Chen, Nanocatalysts for hydrogen generation from ammonia borane and hydrazine borane, *J. Nanomater.*, 2014, **2014**, 4.

6 B. Peng and J. Chen, Ammonia borane as an efficient and lightweight hydrogen storage medium, *Energy Environ. Sci.*, 2008, **1**(4), 479–483.

7 U. B. Demirci and P. Miele, Sodium borohydride *versus* ammonia borane, in hydrogen storage and direct fuel cell applications, *Energy Environ. Sci.*, 2009, **2**, 627–637.

8 Z. H. Lu and Q. Xu, Recent progress in boron-and nitrogen-based chemical hydrogen storage, *Funct. Mater. Lett.*, 2012, **5**(01), 1230001.

9 M. Yadav and Q. Xu, Liquid-phase chemical hydrogen storage materials, *Energy Environ. Sci.*, 2012, **5**(12), 9698–9725.

10 H. Wu, M. Wu, B. Wang, X. Yong, Y. Liu, B. Li, B. Liu and S. Lu, Interface electron collaborative migration of Co-Co3O4/carbon dots: boosting the hydrolytic dehydrogenation of ammonia borane, *J. Energy Chem.*, 2020, **48**, 43–53.

11 Y. Liu, X. Yong, Z. Liu, Z. Chen, Z. Kang and S. Lu, Unified catalyst for efficient and stable hydrogen production by both the electrolysis of water and the hydrolysis of ammonia borane, *Adv. Sustainable Syst.*, 2019, **3**(5), 1800161.

12 Z. Wei, Y. Liu, Z. Peng, H. Song, Z. Liu, B. Liu, B. Li, B. Yang and S. Lu, Cobalt-ruthenium nanoalloys parceled in porous nitrogen-doped graphene as highly efficient difunctional catalysts for hydrogen evolution reaction and hydrolysis of ammonia borane, *ACS Sustain. Chem. Eng.*, 2019, **7**(7), 7014–7023.

13 S. Akbayrak and S. Özkar, Ammonia borane as hydrogen storage materials, *Int. J. Hydrogen Energy*, 2018, **43**(40), 18592–18606.

14 U. Sanyal, U. B. Demirci, B. R. Jagirdar and P. Miele, Hydrolysis of ammonia borane as a hydrogen source: fundamental issues and potential solutions towards implementation, *ChemSusChem*, 2011, **4**(12), 1731–1739.

15 C. Du, Q. Ao, N. Cao, L. Yang, W. Luo and G. Cheng, Facile synthesis of monodisperse ruthenium nanoparticles supported on graphene for hydrogen generation from hydrolysis of ammonia borane, *Int. J. Hydrogen Energy*, 2015, **40**(18), 6180–6187.

16 F. Durap, M. Zahmakıran and S. Özkar, Water soluble laurate-stabilized ruthenium(0) nanoclusters catalyst for hydrogen generation from the hydrolysis of ammonia-borane: high activity and long lifetime, *Int. J. Hydrogen Energy*, 2009, **34**(17), 7223–7230.

17 M. Chandra and Q. Xu, Room temperature hydrogen generation from aqueous ammonia-borane using noble metal nano-clusters as highly active catalysts, *J. Power Sources*, 2007, **168**(1), 135–142.

18 J. Manna, S. Akbayrak and S. Özkar, Palladium(0) nanoparticles supported on polydopamine coated CoFe$_2$O$_4$ as highly active, magnetically isolable and reusable catalyst for hydrogen generation from the hydrolysis of ammonia borane, *Appl. Catal., B*, 2017, **208**, 104–115.

19 S. Akbayrak, Y. Tonbul and S. Özkar, Ceria supported rhodium nanoparticles: superb catalytic activity in hydrogen generation from the hydrolysis of ammonia borane, *Appl. Catal., B*, 2016, **198**, 162–170.

20 L. Zhou, J. Meng, P. Li, Z. Tao, L. Mai and J. Chen, Ultrasmall cobalt nanoparticles supported on nitrogen-doped porous carbon nanowires for hydrogen evolution from ammonia borane, *Mater. Horiz.*, 2017, **4**(2), 268–273.

21 Q. Yao, Z. H. Lu, W. Huang, X. Chen and J. Zhu, High Pt-like activity of the Ni–Mo/graphene catalyst for hydrogen evolution from hydrolysis of ammonia borane, *J. Mater. Chem. A*, 2016, **4**(22), 8579–8583.

22 D. Lu, G. Yu, Y. Li, M. Chen, Y. Pan, L. Zhou, K. Yang, X. Xiong, P. Wu and Q. Xia, RuCo NPs supported on MIL-96 (Al) as highly active catalysts for the hydrolysis of ammonia borane, *J. Alloys Compd.*, 2017, **694**, 662–671.

23 H. Liang, G. Chen, S. Desinan, R. Rosei, F. Rosei and D. Ma, In situ facile synthesis of ruthenium nanocluster catalyst supported on carbon black for hydrogen generation from the hydrolysis of ammonia-borane, *Int. J. Hydrogen Energy*, 2012, **37**(23), 17921–17927.

24 W. Chen, J. Ji, X. Duan, G. Qian, P. Li, X. Zhou, D. Chen and W. Yuan, Unique reactivity in Pt/CNT catalyzed hydrolytic dehydrogenation of ammonia borane, *Chem. Commun.*, 2014, **50**(17), 2142–2144.

25 N. Cao, W. Luo and G. Cheng, One-step synthesis of graphene supported Ru nanoparticles as efficient catalysts for hydrolytic dehydrogenation of ammonia borane, *Int. J. Hydrogen Energy*, 2013, **38**(27), 11964–11972.

26 Q. Yao, W. Shi, G. Feng, Z. H. Lu, X. Zhang, D. Tao, D. Kong and X. Chen, Ultrafine Ru nanoparticles embedded in SiO$_2$ nanospheres: highly efficient catalysts for hydrolytic dehydrogenation of ammonia borane, *J. Power Sources*, 2014, **257**, 293–299.

27 H. Can and Ö. Metin, A facile synthesis of nearly monodisperse ruthenium nanoparticles and their catalysis in the hydrolytic dehydrogenation of ammonia borane for chemical hydrogen storage, *Appl. Catal., B*, 2012, **125**, 304–310.

28 N. Z. Shang, C. Feng, S. T. Gao and C. Wang, Ag/Pd nanoparticles supported on amine-functionalized metal–organic framework for catalytic hydrolysis of ammonia borane, *Int. J. Hydrogen Energy*, 2016, **41**(2), 944–950.

29 H. Chu, N. Li, X. Qiu, Y. Wang, S. Qiu, J. L. Zeng, Y. Zou, F. Xu and L. Sun, Poly (N-vinyl-2-pyrrolidone)-stabilized ruthenium supported on bamboo leaf-derived porous carbon for NH$_3$BH$_3$ hydrolysis, *Int. J. Hydrogen Energy*, 2019, **44**(55), 29255–29262.

30 D. G. Evans and R. C. T. Slade, Structural aspects of layered double hydroxides, in *Layered double hydroxides, structure and bonding*, ed. X. Duan and D. G. Evans, Springer, Berlin, Heidelberg, 2005, 119, pp. 1–87.

31 H. Chu, Y. Zhu, T. Fang, J. Hua, S. Qiu, H. Liu, L. Qin, Q. Wei, Y. Zou, C. Xiang, F. Xu and L. Sun, Solvothermal synthesis of cobalt nickel layered double hydroxides with a three-dimensional nano-petal structure for high-performance supercapacitors, *Sustainable Energy Fuels*, 2020, **4**, 337–346.

32 P. Wang and L. H. Zhu, Preparation of layered double hydroxide (LDHs)-supported gold catalysts and its activity and stability for low-temperature CO oxidation, *Adv. Mater. Res.*, 2011, **396–398**, 841–847.

33 Z. Gao, K. Sasaki and X. Qiu, Structural memory effect of Mg–Al and Zn–Al layered double hydroxides in the presence of different natural humic acids: process and mechanism, *Langmuir*, 2018, **34**(19), 5386–5395.

34 Y. He, J. Fan, J. Feng, C. Luo, P. Yang and D. Li, Pd nanoparticles on hydrotalcite as an efficient catalyst for partial hydrogenation of acetylene: effect of support acidic and basic properties, *J. Catal.*, 2015, **331**, 118–127.

35 J. P. Perdew, K. Burke and M. Ernzerhof, Generalized gradient approximation made simple, *Phys. Rev. Lett.*, 1996, **77**(18), 3865.

36 G. Kresse and J. Furthmüller, Efficiency of *ab initio* total energy calculations for metals and semiconductors using a plane-wave basis set, *Comput. Mater. Sci.*, 1996, **6**(1), 15–50.

37 G. Kresse and J. Furthmüller, Efficient iterative schemes for *ab initio* total-energy calculations using a plane-wave basis set, *Phys. Rev. B*, 1996, **54**(16), 11169.

38 J. P. Perdew, J. A. Chevary, S. H. Vosko, K. A. Jackson, M. R. Pederson, D. J. Singh and C. Fiolhais, Atoms, molecules, solids, and surfaces: applications of the generalized gradient approximation for exchange and correlation, *Phys. Rev. B*, 1992, **46**(11), 6671.

39 J. P. Perdew, K. Burke and M. Ernzerhof, Generalized gradient approximation made simple, *Phys. Rev. Lett.*, 1996, **77**(18), 3865.

40 S. Grimme, Semiempirical GGA-type density functional constructed with a long-range dispersion correction, *J. Comput. Chem.*, 2006, **27**(15), 1787–1799.

41 G. Jiang, W. Fu, S. Shu, Z. Zhang, S. Zhang, Y. Zhang, X. Zhang, F. Dong and X. Lv, MgAl layered double oxide: one powerful sweeper of emulsified water and acid for oil purification, *J. Hazard Mater.*, 2019, **367**, 658–667.

42 G. Chen, R. Wang, W. Zhao, B. Kang, D. Gao, C. Li and J. Y. Lee, Effect of Ru crystal phase on the catalytic activity of hydrolytic dehydrogenation of ammonia borane, *J. Power Sources*, 2018, **396**, 148–154.

43 L. Wen, J. Su, X. Wu, P. Cai, W. Luo and G. Cheng, Ruthenium supported on MIL-96: an efficient catalyst for hydrolytic dehydrogenation of ammonia borane for chemical hydrogen storage, *Int. J. Hydrogen Energy*, 2014, **39**(30), 17129–17135.

44 S. Akbayrak, Y. Tonbul and S. Özkar, Ceria-supported ruthenium nanoparticles as highly active and long-lived catalysts in hydrogen generation from the hydrolysis of ammonia borane, *Dalton Trans.*, 2016, **45**(27), 10969–10978.

45 X. Wang, D. Liu, S. Song and H. Zhang, Synthesis of highly active Pt–CeO₂ hybrids with tunable secondary nanostructures for the catalytic hydrolysis of ammonia borane, *Chem. Commun.*, 2012, **48**(82), 10207–10209.

46 J. Manna, S. Akbayrak and S. Özkar, Palladium(0) nanoparticles supported on polydopamine coated CoFe₂O₄ as highly active, magnetically isolable and reusable catalyst for hydrogen generation from the hydrolysis of ammonia borane, *Appl. Catal., B*, 2017, **208**, 104–115.

47 Y. Wu, X. Wu, Q. Liu, C. Huang and X. Qiu, Magnetically recyclable Ni@h-BN composites for efficient hydrolysis of ammonia borane, *Int. J. Hydrogen Energy*, 2017, **42**(25), 16003–16011.

48 O. Metin, V. Mazumder, S. Ozkar and S. Sun, Monodisperse nickel nanoparticles and their catalysis in hydrolytic dehydrogenation of ammonia borane, *J. Am. Chem. Soc.*, 2010, **132**(5), 1468–1469.

49 Q. Xu and M. Chandra, Catalytic activities of non-noble metals for hydrogen generation from aqueous ammonia–borane at room temperature, *J. Power Sources*, 2006, **163**(1), 364–370.

50 L. Yang, N. Cao, C. Du, H. Dai, K. Hu, W. Luo and G. Cheng, Graphene supported cobalt(0) nanoparticles for hydrolysis of ammonia borane, *Mater. Lett.*, 2014, **115**, 113–116.

51 H. Chu, N. Li, S. Qiu, Y. Zou, C. Xiang, F. Xu and L. Sun, Ruthenium supported on nitrogen-doped porous carbon for catalytic hydrogen generation from NH₃BH₃ hydrolysis, *Int. J. Hydrogen Energy*, 2019, **44**(3), 1774–1781.

52 Y. Lin, L. Yang, H. Jiang, Y. Lin, L. Yang, H. Jiang, Y. Zhang, D. Cao, C. Wu and L. Song, Boosted reactivity of ammonia borane dehydrogenation over Ni/Ni₂P heterostructure, *J. Phys. Chem. Lett.*, 2019, **10**(5), 1048–1054.

53 C. Wang, J. Tuninetti, Z. Wang, C. Zhang, R. Ciganda, L. Salmon, S. Moya, J. Ruiz and D. Astruc, Hydrolysis of ammonia-borane over Ni/ZIF-8 nanocatalyst: high efficiency, mechanism, and controlled hydrogen release, *J. Am. Chem. Soc.*, 2017, **139**(33), 11610–11615.

54 C. C. Hou, Q. Li, C. J. Wang, C. Y. Peng, Q. Q. Chen, H. F. Ye, W. F. Fu, C. M. Che, N. López and Y. Chen, Ternary Ni-Co-P nanoparticles as noble-metal-free catalysts to boost the hydrolytic dehydrogenation of ammonia-borane, *Energy Environ. Sci.*, 2017, **10**(8), 1770–1776.

55 W. Zhao, R. Wang, Y. Wang, J. Feng, C. Li and G. Chen, Effect of LDH composition on the catalytic activity of Ru/LDH for the hydrolytic dehydrogenation of ammonia borane, *Int. J. Hydrogen Energy*, 2019, **44**(29), 14820–14830.